

# Internal Motion of 6.7-GHz Methanol Masers in H II Region S269

Satoko SAWADA-SATOH<sup>1</sup> Kenta FUJISAWA<sup>2</sup> Koichiro SUGIYAMA<sup>2</sup> Kiyooki WAJIMA<sup>2,3</sup> Mareki HONMA<sup>4,5</sup>

<sup>1</sup>*Mizusawa VLBI Observatory, National Astronomical Observatory of Japan,  
2-12 Hoshigaoka-cho, Mizusawa-ku, Oshu, Iwate 023-0861*

*satoko.ss@nao.ac.jp*

<sup>2</sup>*Graduate school of Science and Engineering, Yamaguchi University,  
1677-1 Yoshida, Yamaguchi, Yamaguchi 753-8512*

<sup>3</sup>*Shanghai Astronomical Observatory, Chinese Academy of Sciences, 80 Nandan Road, Shanghai 200030, China*

<sup>4</sup>*National Astronomical Observatory of Japan, 2-21-1 Osawa, Mitaka, Tokyo 181-8588*

<sup>5</sup>*Department of Astronomy, Graduate University for Advanced Studies, 2-21-1 Osawa, Mitaka, Tokyo 181-8588*

(Received 2013 January 9; accepted 2013 March 25)

## Abstract

We present the first internal motion measurement of the 6.7-GHz methanol maser within S269, a small H II region in the outer Galaxy, which was carried out in 2006 and 2011 using the Japanese VLBI Network (JVN). Several maser groups and weak isolated spots were detected in an area spanning by  $\sim 200$  mas (1000 AU). Three remarkable maser groups are aligned at a position angle of  $80^\circ$ . Two of three maser groups were also detected by a previous observation in 1998, which allowed us to study a long-term position variation of maser spots from 1998 to 2011. The angular separation between the two groups increased  $\sim 10$  mas, which corresponds to an expansion velocity of  $\sim 10$  km s<sup>-1</sup>. Some velocity gradient ( $\sim 10^{-2}$  km s<sup>-1</sup> mas<sup>-1</sup>) in the overall distribution was found. The internal motion between the maser groups support the hypothesis that the methanol masers in S269 could trace a bipolar outflow.

**Key words:** IMS: H II regions — ISM:individual (S269) — stars: formation — masers:methanol

## 1. Introduction

The  $5_1 \rightarrow 6_0 A^+$  methanol maser transition near 6.7 GHz discovered by Menten (1991) is known to be closely associated with high-mass star-forming regions (e.g. Caswell et al. 1995; Walsh et al. 1997; Minier et al. 2003; Xu et al. 2008). They are thought to be a probe of just before and/or after the onset of the ultra compact (UC) H II region (e.g., Walsh et al. 1998).

Various morphologies of the 6.7 GHz methanol masers have been obtained with past interferometric and VLBI observations. The linear distribution and velocity gradient of the masers have often been explained as an edge-on rotation disk (e.g. Norris et al. 1998). Such a rotation disk hypothesis is supported by detections of internal motions surrounding a radio continuum source (Sanna et al. 2010a; Sanna et al. 2010b; Goddi et al. 2011; Moscadelli et al. 2011). Moreover, several ring-like distributions of masers have been applied to a disk model with rotation plus expansion/infall motion (e.g. Bartkiewicz et al. 2005; Bartkiewicz et al. 2009; Sugiyama et al. 2008b; Torstensson et al. 2011). However, De Buizer et al. (2012) resolved the near- and mid-infrared emission at the locations of four methanol maser rings, and did not find consistent morphology of IR emission based on the hypothesis that the masers reside in the circumstellar disks.

On the other hand, a shock-wave model has been presented to explain the maser location in several sources (Phillips et al. 1998; Walsh et al. 1998; Dodson et al. 2004). De Buizer (2003) searched for H<sub>2</sub> out-

flow signatures in massive young stellar objects with the linear distribution of methanol masers to test whether the outflows are perpendicular to the linear distributions. Their search revealed that H<sub>2</sub> emission is distributed almost parallel to the distribution of methanol masers in their sample sources. In addition, multi-epoch VLBI observations have shown the internal motions of methanol masers in massive star-forming region ON1, which suggested that the masers trace the expansion of the UC H II region or a bipolar outflow (Rygl et al. 2010; Sugiyama et al. 2011). The 6.7 GHz methanol maser emission has been detected on size scale of 1000 AU from young stellar objects, and can be a powerful tool to investigate the environment close to the forming high-mass protostar. However, internal motions of the 6.7 GHz methanol masers have been reported in limited number of sources so far (e.g. G16.59-0.05 for Sanna et al. 2010a; G23.01-0.41 for Sanna et al. 2010b; ON1 for Rygl et al. 2010; Sugiyama et al. 2011; IRAS 20126+4104 for Moscadelli et al. 2011; W3(OH) for Matsumoto et al. 2011; AFGL 5142 for Goddi et al. 2011).

S269 (G196.45-1.68) is a small H II region spanning about  $2'$  (Heydari-Malayeri et al. 1982), which is located in the outer Galaxy. S269 harbors two bright near-infrared (IR) sources separated by  $\sim 30''$ , IRS 1 and IRS 2 (Wynn-Williams et al. 1974a). Later, IRS 2 was resolved into double sources IRS 2e and IRS 2w with a separation of  $4''$  (Eiroa et al. 1994; Eiroa & Casali 1995). Recent near-IR images imply that several H<sub>2</sub> knots are distributed across IRS2, which suggest two bipolar out-

**Table 1.** Observation parameters

Epoch	Date [yyyy/mm/dd]	Telescopes*	Synthesized beam [mas, mas, degree]	On-source time [hr]	$I_{\text{rms}}^{\dagger}$ [mJy beam <sup>-1</sup> ]
1	2006/09/10	Y, U, M, I	23×3, -34	2.1	110
2	2011/10/22	Y, U, H, M, R, O, I	8×3, -46	6.5	10

\* Telescope code — Y: Yamaguchi, U: Usuda, H: Hitachi, M: VERA-Mizusawa, R: VERA-Iriki, O: VERA-Ogasawara, I: VERA-Ishigaki.

<sup>†</sup> Image rms noise level for line-free channel map.

flows, powered by sources in IRS 2 (Jiang et al. 2003). In S269, several signposts of star-forming activities such as OH and H<sub>2</sub>O masers (e.g. Wynn-Williams et al. 1974b; Genzel & Downes 1977), high-velocity CO wing emission (Wouterloot & Brand 1989; Yang et al. 2002) and a Herbig-Haro object (Eiroa et al. 1994) have been detected.

The 6.7-GHz methanol maser emission has been also found in S269 (Menten 1991; Szymczak, Hrynek & Kus 2000). The monitoring observations of 6.7-GHz methanol maser emission from 1999 to 2003 revealed that the three main methanol maser features have a sinusoidal time variation with a period of 668 days (Goedhart et al. 2004). From past VLBI observation of 6.7-GHz methanol masers in S269 using the European VLBI Network (EVN), Minier et al.(2000, hereafter M00) detected two maser groups named A and B; there is a single maser spot at velocity of 14.70 km s<sup>-1</sup> in group A, and eight maser spots at a velocity range of 15.04–15.43 km s<sup>-1</sup> distributed in a linear structure of  $\sim 15$  mas at southeast–northwest direction with a clear velocity gradient in group B. The VLBI image by M00 showed that two groups were separated by  $\sim 55$  mas in 1998 November, and suggested that the methanol masers are probably associated with IRS 2. Recent astrometric observation of water maser in S269 with VERA also revealed that the absolute position of the water maser feature agrees well with the position of IRS 2w (Honma et al. 2007).

In this paper, we present 6.7-GHz methanol maser images of S269, eight and thirteen years after the past VLBI observation by M00, and report the first measurements of the internal motion of the S269 methanol maser. We adopt  $D = 5.28$  kpc to S269 (Honma et al. 2007), and hence 1 mas corresponds to 5.27 AU.

## 2. Observations and Data Reduction

VLBI observations of 6.7-GHz methanol masers in S269 were carried out at two epochs, on 2006 September 10 using four telescopes of the Japanese VLBI Network (JVN), and on 2011 October 22 using seven telescopes (table 1). At Epoch 1, left-circular polarization was received at Yamaguchi and Usuda, while linear polarization was received at VERA Mizusawa and VERA Ishigaki. At Epoch 2, left-circular polarization was received at all telescopes. The data were recorded with the VSOP terminal system (Kawaguchi et al. 1994). The recorded data were correlated with the Mitaka FX correlator (Shibata et al. 1998).

Data reduction including calibration, data flagging, fringe fitting and imaging utilized using the NRAO AIPS

package. For visibility-amplitude calibration, we applied the “template method” (e.g. Diamond 1995) in order to correct any short term gain fluctuations and pointing errors with a time resolution of 30 seconds.

We corrected the visibility amplitude decrement due to the correlation between different (circular- or linear-) polarization data at Epoch 1 under assumption of no significant polarization of the source, using the method of Sugiyama et al.(2008a). A visibility amplitude in correlation between circular- and linear- polarization data reduces by  $1/\sqrt{2}$ . For the case of visibility amplitude in correlation between linear- and linear- polarization data, the amplitude varies with time of observation, or parallactic angle of observing source at the time. We applied the amplitude correction factor for each baseline visibility.

The residual delays and rates were estimated from observations of the continuum source 0611+131. The bandpass responses were calibrated with observations of 4C39.25. Fringe fitting and self calibration were done for the brightest methanol maser emission in S269. Channel maps were made every 0.178 km s<sup>-1</sup> with uniform weighting. The positions of the detected maser spots were derived by fitting an elliptical Gaussian brightness distribution to the maps using the AIPS task JMFIT. The observation parameters for the JVN observations are summarized in table 1.

We have also carried out the single-dish observations toward the 6.7-GHz methanol maser emission of S269 with the Yamaguchi 32-m telescope almost simultaneously with each JVN observation, for an absolute flux calibration to the VLBI data. The observations were performed for four days from 2006 September 4, and one day on 2011 October 22 just after the JVN observations toward S269.

The dual circular polarizations were recorded simultaneously, and combined after being transformed into the spectra. The velocity resolution was 0.044 km s<sup>-1</sup>. The integration time was 14 minutes for each day, and the rms noise level was typically 1.0 Jy for one spectral channel. Spectral profile in September 2006 was obtained by averaging the four-day data, resulting the rms noise level of 0.5 Jy. Amplitude and gain calibrations were performed with the use of noise-sources having known noise temperatures.

## 3. Results

### 3.1. Spectra

Spectral profiles of the 6.7-GHz methanol maser emission in S269 are shown in figure 1. The maser emission was detected at velocity range of 14.0–16.5 km s<sup>-1</sup>. The

**Table 2.** Flux densities of the 6.7-GHz methanol maser peaks

$V_{\text{LSR}}$ [ $\text{km s}^{-1}$ ]	Flux density	
	2006 September	2011 October
	[Jy]	
14.7	9.8	21.1
15.2	19.0	22.8
15.9	6.1	14.1

spectrum detected with the Yamaguchi 32-m telescope revealed the brightest peak at velocity of  $15.2 \text{ km s}^{-1}$ , and blue-shifted and red-shifted spectral components at peak velocities of  $14.7$  and  $15.9 \text{ km s}^{-1}$ , which is consistent with the past single-dish observations (Szymczak, Hrynek & Kus 2000; Goedhart et al. 2004). The flux densities at the peaks of  $14.7$ ,  $15.2$  and  $15.9 \text{ km s}^{-1}$  are summarized in table 2. The values of the peak flux densities in 2006 lie within the variation range ( $20\text{--}50 \text{ Jy}$  at  $15.2 \text{ km s}^{-1}$ ,  $0\text{--}10 \text{ Jy}$  at  $14.7$  and  $15.9 \text{ km s}^{-1}$ ) observed during the period from 1999 January to 2003 March by single-dish monitoring (Goedhart et al. 2004). In 2011, the peak flux densities at  $14.7$  and  $15.9 \text{ km s}^{-1}$  rise up over the variation range, while the peak value at  $15.2 \text{ km s}^{-1}$  is close to the value at its minimum intensity. This variation is different from the behavior during the period of the past monitoring observations.

### 3.2. Spatial distributions

Figure 2 shows the 6.7-GHz methanol maser distribution in S269. At both of Epoch 1 and 2, all maser spots distribute over a range of  $\sim 200 \text{ mas}$  ( $1000 \text{ AU}$ ). The maser distribution is organized by several maser groups and some weak isolated spots. Here, we give labels to remarkable groups (A, B, C, D and E). Groups A, B and C are seen at both Epoch 1 and 2, and aligned along the direction at a position angle of  $\sim 80^\circ$ .

The most luminous maser spot at  $15.2 \text{ km s}^{-1}$  belongs to group B. The maser spots in group B distribute in a linear structure of  $\sim 10 \text{ mas}$  in the southeast–northwest direction with a velocity gradient. The maser distribution of group B in 1998 by M00 show a similar linear structure of  $\sim 14 \text{ mas}$  in the southeast–northwest direction, and the size became smaller. The velocity ranges of detected maser spots in group B were similar in 1998 and 2006 (Epoch 1);  $15.04$  to  $15.43 \text{ km s}^{-1}$  in 1998 and  $15.02$  to  $15.55 \text{ km s}^{-1}$  in 2006. At Epoch 2, the velocity range of group B was broadened to  $15.00\text{--}16.16 \text{ km s}^{-1}$  and several spots at  $15.67\text{--}16.16 \text{ km s}^{-1}$  are newly detected. In 2011, the structure of group B is still elongated, but its velocity gradient became less simple.

Group A is the second brightest, which locates at  $\sim 55 \text{ mas}$  east from group B. At Epoch 1, it consists of two maser spots at velocities of  $14.67$  and  $14.85 \text{ km s}^{-1}$  with an angular separation of  $\sim 1 \text{ mas}$ . Its compact structure and velocity range agree well with the past VLBI observations in 1998 by M00. At Epoch 2, however, four spots with a velocity range of  $14.84$  to  $15.33 \text{ km s}^{-1}$  are linearly

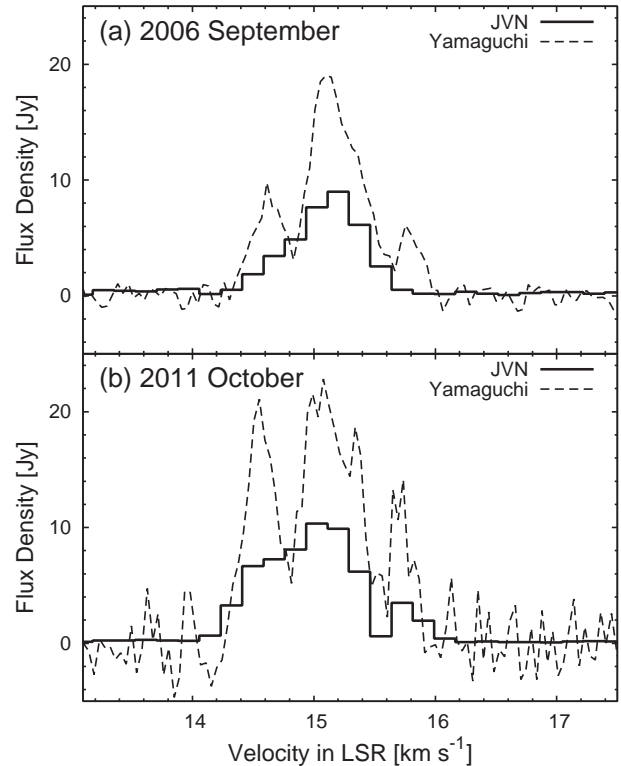


**Fig. 1.** Comparison of the cross-power spectrum (vector average) obtained from our JVN observations (Solid line) and the spectral profile measured with the Yamaguchi 32-m telescope (Dashed line). Velocity resolution is  $0.178 \text{ km s}^{-1}$  and  $0.044 \text{ km s}^{-1}$ , respectively. (a) Spectra in 2006 September. The spectral profile measured with the Yamaguchi 32-m telescope is obtained by averaging spectra observed from 2006 September 4 to 7. (b) Spectra in 2011 October 22.

distributed over  $\sim 10 \text{ mas}$  with a clear velocity gradient.

Group C is located  $95 \text{ mas}$  west from group B. It is divided into two spectral channels at velocities of  $15.73$  and  $15.91 \text{ km s}^{-1}$  at Epoch 1, while it consists of three maser spots at velocities of  $16.33$  and  $16.49 \text{ km s}^{-1}$  at Epoch 2. We cannot identify the detected maser spots within group C in the two epochs as being the same, because there is a difference of  $\sim 0.5 \text{ km s}^{-1}$  in velocity, larger than the velocity resolution of  $0.178 \text{ km s}^{-1}$ , between two epochs in their LSR velocities.

At Epoch 2, two prominent maser groups (labeled D and E in figure 2b and table 3) are visible. Group D is seen at  $70 \text{ mas}$  west and  $60 \text{ mas}$  north from group B. Group D consists of several maser spots with velocities of  $16.00$  and  $16.17 \text{ km s}^{-1}$ . The appearance of group D is consistent with brightening of the maser peak at  $15.9 \text{ km s}^{-1}$  in the spectral profile (figure 1b). Group E consists of several blueshifted maser spots at velocities of  $14.8\text{--}15.3 \text{ km s}^{-1}$ , and its detection is in accord with the brightening of the maser peak at  $14.7 \text{ km s}^{-1}$ . They are framed in by a dotted rounded box in figure 2b, and distributed over  $\sim 170 \text{ mas}$  on the dashed line at a position angle of  $125^\circ$  in figure 2b, almost parallel to the alignment direction of the  $\text{H}_2$  knots 1,2,3,4 and 5. The maser spots in group B

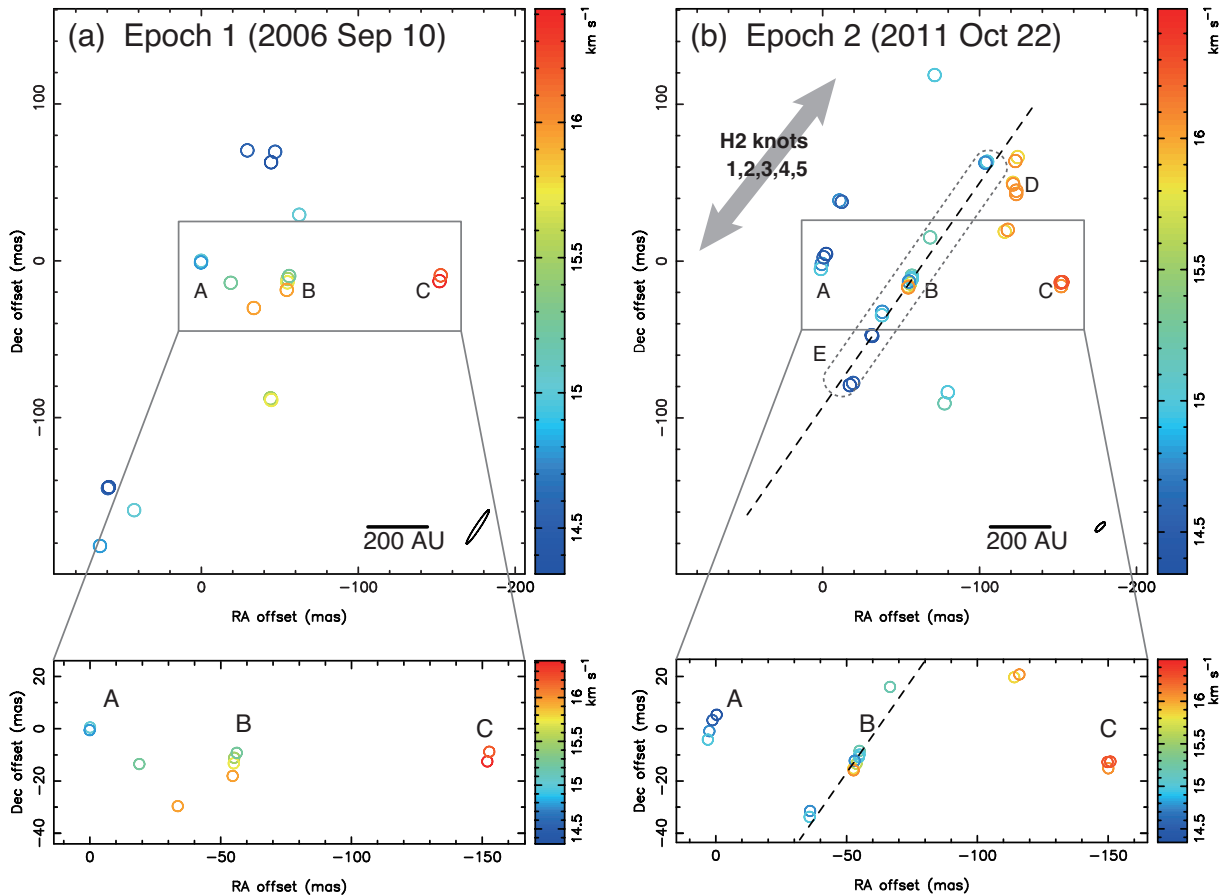


**Fig. 2.** The 6.7-GHz methanol maser distribution, observed with the JVN on (a) 2006 September 10 and (b) 2011 October 22. Color circles mark maser spots detected at the  $>10\sigma$  level in a single channel, or detected at the  $>7\sigma$  level in two adjacent channels with the position overlapping within the beam size. Color indicates the LSR doppler velocity of the spectral channel. The synthesized beam size is shown at the lower right in wide-field view. In (b), the dashed lines indicate the direction at position angle of  $125^\circ$ , and a grey arrow represents the direction of alignment for the  $H_2$  knots 1, 2, 3, 4 and 5 (Jiang et al. 2003).

and E seem to be aligned on the same line in the direction at position angle of  $125^\circ$ . The two maser groups D and E are brighter than group C, but not as bright as group A.

The maser spots, except groups A and B were not visible in the EVN observations in 1998 November (M00). The maser peaks at  $14.7$  and  $15.9$   $\text{km s}^{-1}$  could be at the minimum phase in intensity at that time, as Goedhart et al. (2004) has shown.

### 3.3. Internal motion

Since we did not use the technique of phase referencing for our VLBI observations, the absolute information of position is unknown. Furthermore, there is uncertainty about the identification of each maser spot, because (i) the different velocity resolutions between EVN and JVN; and (ii) time variation of velocity ranges of groups A, B and C at Epoch 2. Therefore, we here describe the relative position of the maser spots with respect to the barycentric point among maser spots within group A for each epoch. For 1998, the reference point is the position of the single maser spot at a velocity of  $14.70$   $\text{km s}^{-1}$  in group A.

The relative positions of the maser spots in groups A, B and C are listed in table 4. The superposition of the

maser distributions in 1998 (M00), 2006 (Epoch 1) and 2011 (Epoch 2) is shown in figure 3. The spatial and velocity structure of groups A, B are similar during the period from 1998 to 2011. Group C appears in 2006 (Epoch 1) and 2011 (Epoch 2), and there are similarities concerning the position and the compactness of its structure between the two epochs. The angular separation between the barycentric points of groups A and B increases 5 mas for thirteen years from 1998 to 2011. If we assume that it increases at a constant rate, the velocity of the internal motion is estimated to be  $10$   $\text{km s}^{-1}$ . We note that the maser distribution and the velocity range of group A at Epoch 2 are changed from two previous VLBI observations in 1998 and 2006 (Epoch 1), and there could be uncertainty about the reference point at Epoch 2. If we exclude the results at Epoch 2 for estimation of the internal motion between group A and B, the velocity of the motion would be calculated to be  $13$   $\text{km s}^{-1}$ , since the angular separation increases by 4 mas from 1998 to 2006.

It is difficult to discuss about the motion of group C, because the velocity range of group C at Epoch 1 and 2 is not same, and therefore the maser spots in group C in different epochs cannot be identified as being the same.

**Table 3.** Parameters of maser spots in group D and E at Epoch 2

$V_{\text{LSR}}$ [km s $^{-1}$ ]	Relative RA*	Relative Dec*	Peak Intensities [Jy beam $^{-1}$ ]
	[mas]		
Group D			
16.00	-115.66	18.78	0.50
16.00	-120.91	49.77	0.38
16.00	-123.90	66.23	0.32
16.16	-117.62	19.86	0.32
16.16	-121.06	48.82	0.29
16.16	-122.47	63.70	0.26
16.16	-123.01	42.72	0.27
16.16	-123.05	44.84	0.26
Group E			
14.84	-17.03	-79.03	0.34
14.84	-31.28	-47.72	0.33
15.00	-19.16	-77.65	0.45
15.00	-30.91	-47.19	0.46
15.17	-37.65	-32.30	0.50
15.17	-120.91	49.77	0.38
15.33	-37.48	-34.57	0.47
15.33	-104.48	63.27	0.41
15.50	-68.20	15.10	0.44

\* Relative position with respect to the barycentric point of group A.

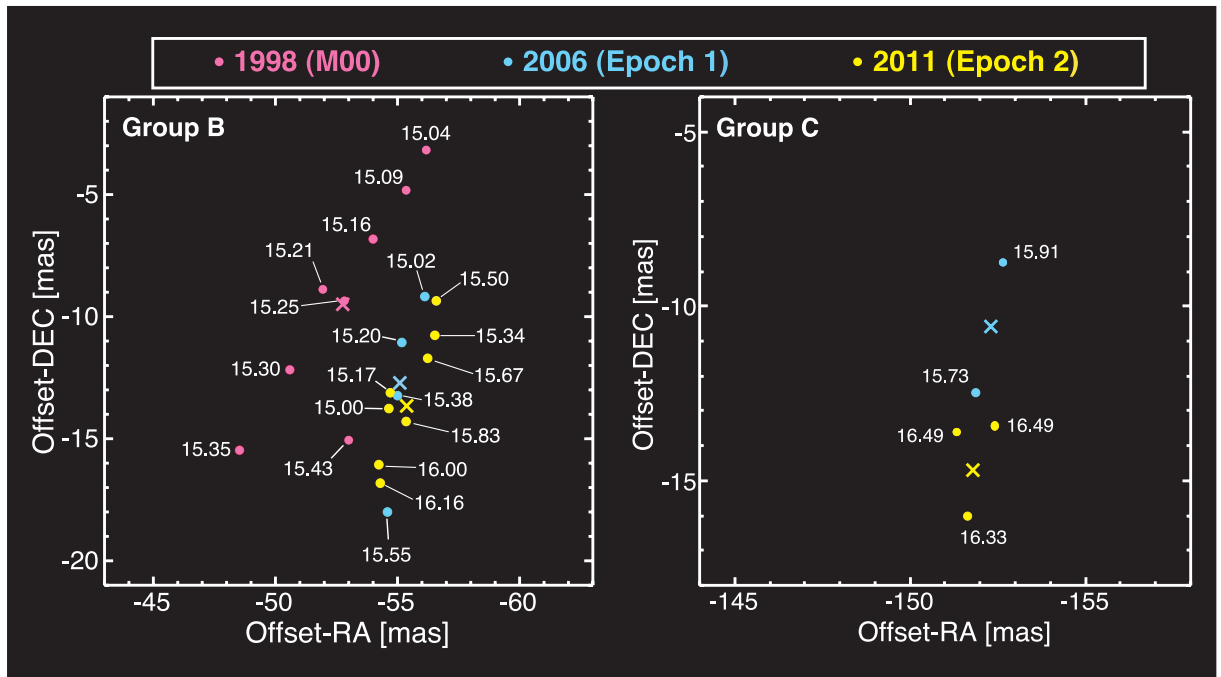


**Fig. 3.** Superposed maps of the 6.7-GHz methanol maser distribution in groups B and C with respect to group A in 1998 (M00), 2006 (Epoch 1) and 2011 (Epoch 2). Color circles mark the maser spots, and a cross represents the barycentric point for each group and epoch. The coordinate origin (0,0) is set to the barycentric point among maser spots within group A for each epoch. For 1998, the origin (0,0) is the position of the single maser spot at a velocity of 14.70 km s $^{-1}$  in group A.

**Table 4.** Positions of the maser spots in group A, B and C

Group	$V_{\text{LSR}}$ [ $\text{km s}^{-1}$ ]	Relative RA*	Relative Dec*
		[mas]	[mas]
1998 (M00)			
A	14.70	0.00	0.00
B	15.04	-56.15	-3.17
B	15.09	-55.35	-4.89
B	15.16	-54.01	-6.81
B	15.21	-51.93	-8.89
B	15.25	-52.80	-9.35
B	15.30	-50.59	-12.16
B	15.35	-48.54	-15.47
B	15.43	-53.00	-15.03
2006 (Epoch 1)			
A	14.67	0.08	-0.51
A	14.85	-0.08	0.51
B	15.02	-56.13	-9.18
B	15.20	-55.19	-11.06
B	15.38	-54.99	-13.20
B	15.55	-54.57	-18.00
C	15.73	-151.88	-12.46
C	15.91	-152.64	-8.75
2011 (Epoch 2)			
A	14.84	-1.93	4.47
A	15.00	-0.35	2.38
A	15.17	0.86	-1.81
A	15.34	1.43	-5.04
B	15.00	-54.65	-13.74
B	15.17	-54.68	-13.10
B	15.34	-56.29	-11.65
B	15.50	-56.56	-9.34
B	15.67	-56.24	-11.68
B	15.83	-55.36	-14.27
B	16.00	-54.22	-16.08
B	16.16	-54.29	-16.78
C	16.33	-152.42	-13.42
C	16.49	-151.31	-13.60
C	16.49	-151.62	-16.01

\* Relative position with respect to the barycentric point of group A.

### 3.4. Velocity gradient

The velocity gradient in the overall distribution could roughly be seen along the alignment of groups A, B and C at a position angle of  $\sim 80^\circ$ . At Epoch 2, another obvious linear structure, which consists of groups B and E, is seen along the southeast–northwest direction (position angle of  $125^\circ$ ) in figure 2. However, a more rigorous inspection for the individual maser groups indicates that the velocity gradient is not simple. A position-velocity diagram along the direction at position angles of  $80^\circ$  and  $125^\circ$  indicates a linear fitting of velocity gradient of  $9.5 \text{ m s}^{-1} \text{ mas}^{-1}$  and  $6.4 \text{ m s}^{-1} \text{ mas}^{-1}$ , respectively (figure 4).

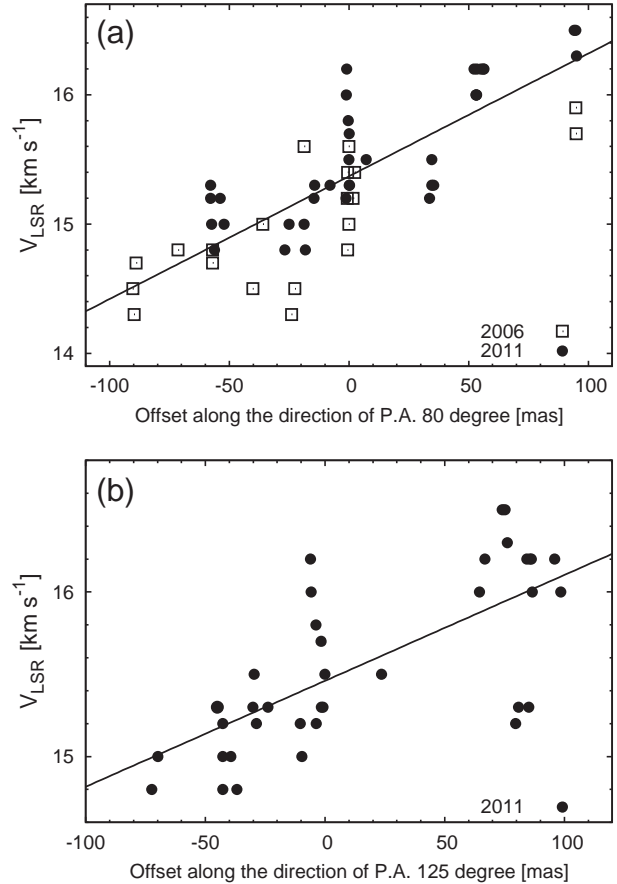


**Fig. 4.** (a) Position-Velocity diagram of all the maser spots detected in 2006 and 2011, along the direction at position angle of  $80^\circ$ . The open square and the filled circle indicates the maser spots obtained from VLBI observations in 2006 and 2011, respectively. The solid line represents a linear fit and indicates a velocity gradient of  $9.5 \text{ m s}^{-1} \text{ mas}^{-1}$ . (b) Position-Velocity diagram of all the maser spots detected in 2011 along the direction at position angle of  $125^\circ$ . The solid line represents a linear fit and indicates a velocity gradient of  $6.4 \text{ m s}^{-1} \text{ mas}^{-1}$ .

## 4. Discussions

As described in introduction, the 6.7-GHz methanol maser emission has been considered to trace various structures in high-mass star-forming region. Here, we discuss possible scenarios where 6.7-GHz methanol maser emission is associated with a bipolar outflow or a disk.

### 4.1. Outflow scenario

The bipolar outflow scenario is the simplest explanation for the increase of the angular separation between two maser groups A and B. The axis of outflow would be a line joining the two maser groups A and B, in the direction at position angle of  $\sim 80^\circ$ . A possible schematic diagram of the outflow model is shown in figure 5. The viewing angle of the outflow ( $\theta_v$ ) is estimated to be  $87^\circ$ , from the projected relative velocity of  $13 \text{ km s}^{-1}$  ( $V_f \sin \theta_v$ ) and the velocity difference between groups A and B of  $0.6 \text{ km s}^{-1}$  ( $V_f \cos \theta_v$ ). Therefore, the outflow axis is almost parallel to

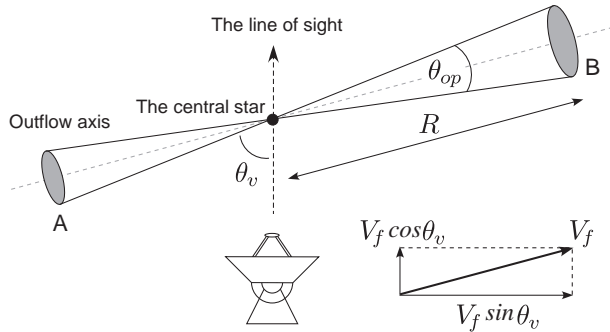


**Fig. 5.** Possible schematic diagram of outflow model to explain the increase of the angular separation between two maser groups, A and B. Groups A and B travel away at the outflow velocity of  $V_f$  from the central star.

the sky plane, and the absolute velocity of the expansion between groups A and B is estimated to be nearly  $13 \text{ km s}^{-1}$ . We derived the momentum rate of the outflow  $\dot{P}_f$ , defined as

$$\dot{P}_f = 2\Omega_f R^2 n_{\text{H}_2} m_{\text{H}_2} V_f^2, \quad (1)$$

where  $\Omega_f$  is the solid angle of the outflow,  $R$  is the distance from the central star,  $n_{\text{H}_2}$  and  $m_{\text{H}_2}$  are the number density, and the weight of molecular hydrogen, and  $V_f$  is the outflow velocity (e.g. Nagayama et al. 2008). The location of the central star would be somewhere on the line segment between groups A and B. The solid angle of the outflow,  $\Omega_f$  is  $2\pi\{1 - \cos(\theta_{op}/2)\}$ , and the opening angle of the outflow,  $\theta_{op}$ , is an appearance angle of group A or B from the central star. Here, we assume that the central star is located at the midpoint between the groups A and B. We obtain  $\dot{P}_f = 2.1 \times 10^{-5} M_\odot \text{ km s}^{-1} \text{ yr}^{-1}$ , adopting  $\theta_{op} = 10^\circ$  as the appearance angle of group A or B from the midpoint that  $V_f = 6.5 \text{ km s}^{-1}$  as half of the absolute velocity of the expansion between groups A and B,  $R = 150 \text{ AU}$  as half of the distance between groups A and B, and a typical gas density for methanol maser environment  $n_{\text{H}_2} = 10^8 \text{ cm}^{-3}$  (Cragg et al. 2005).

Group C is also located on the extension of the line, and groups A, B and C could be associated with the same outflow. However, the direction at a position angle of  $\sim 80^\circ$  is not consistent with a large-scale bipolar outflow in the southeast–northwest direction traced by several  $\text{H}_2$  knots (Knots 1,2,3,4,5; Jiang et al. 2003). Therefore, the internal motion of groups A and B could be driven by another outflow. The near-IR images have suggested the existence of a second outflow with a different axis traced by  $\text{H}_2$  knot 6 as well (Jiang et al. 2003). If the second outflow is powered by sources in IRS 2, the outflow axis would be a line to connect IRS 2 and  $\text{H}_2$  knot 6. We note that the direction of the outflow axis is nearly parallel to the position angle of  $80^\circ$ , which is the alignment of maser groups A, B and C. Currently, there is no strong observational support to link the outflow in southeast–northwest direction traced by several  $\text{H}_2$  knots with the maser spots in group B and E aligned along the direction at position angle of  $125^\circ$  seen at Epoch 2. Measurements of the absolute positions

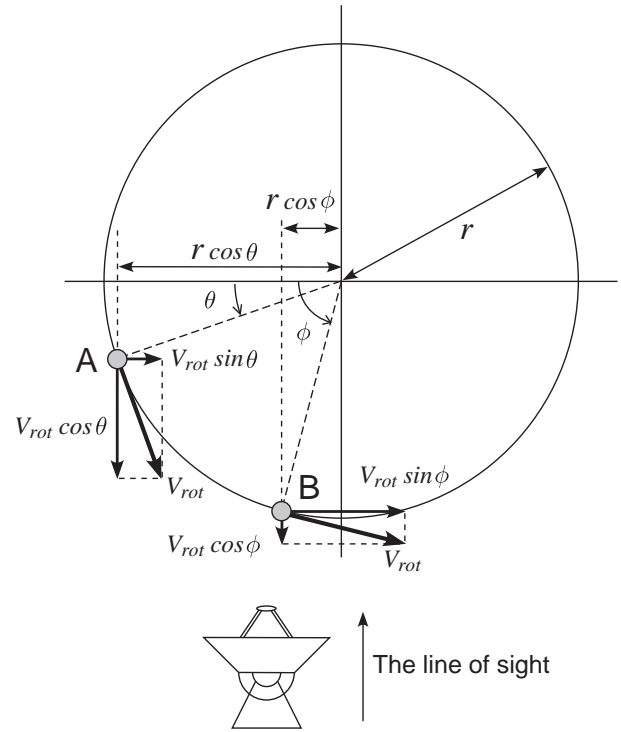


**Fig. 6.** Diagram of a rotation disk from the face-on view. Here, we assume that the maser groups A and B rotate in an orbit with the radius of  $r$  at the rotation velocity of  $V_{rot}$ .

and proper motions of the methanol masers are necessary in order to confirm the relation between the maser spots and the  $\text{H}_2$  knots in southeast–northwest direction.

#### 4.2. Disk scenario

The disk scenario has often been proposed to interpret the maser distribution in a linear distribution with a velocity gradient, and could be another candidate to explain the observational results of the methanol masers. If the velocity gradient of the methanol maser emission is due to a rotation disk, the enclosed mass in the Keplerian law is estimated to be  $\sim 1M_\odot$ , assuming an edge-on view of the disk with a disk radius of  $1000 \text{ AU}$ , the total extent of the methanol masers. The estimated value is too small as a high-mass star forming region, in which 6.7-GHz methanol maser emission is exhibited. This fact has already been pointed out by M00, which suggested the possibility that methanol masers are associated with a fraction of the rotation disk, resulting in an underestimate of the enclosed mass.

Here, we consider the hypothesis that the methanol masers could trace the partial disk, assuming that groups A and B rotate around a protostar in an orbit with a radius of  $r$  at a rotation velocity of  $V_{rot}$ , as shown in figure 6. The projected distance between groups A and B ( $D_{AB} = r \cos \theta - r \cos \phi$ ), the velocity of the relative motion between groups A and B ( $V_{rel} = V_{rot} \sin \phi - V_{rot} \sin \theta$ ), and the difference of the radial velocity between groups A and B ( $\Delta V_{rad} = V_{rot} \cos \theta - V_{rot} \cos \phi$ ) are provided from our VLBI observations. If we assume that groups A and

B are located in the near side of the disk ( $0^\circ \leq \theta \leq 180^\circ$  and  $0^\circ \leq \phi \leq 180^\circ$ ), the orbit radius and the rotation velocity are estimated to be  $r \sim 75000$  AU and  $V_{rot} \sim 150$  km s $^{-1}$ , adopting the observational results:  $D_{AB}$  of 300 AU,  $V_{rel}$  of 13 km s $^{-1}$  and  $\Delta V_{rad}$  of 0.6 km s $^{-1}$ . Using the estimated  $r$  and  $V_{rot}$ , the resulting enclosed mass is  $1.9 \times 10^6 M_\odot$ , which makes this scenario unlikely. If the location of group A is allowed to be at the far side of the disk ( $-180^\circ \leq \theta \leq 0^\circ$ ), much smaller values of the enclosed mass can be derived. When  $(\theta, \phi)$  is  $(-88^\circ, 92^\circ)$ , the minimum value of the enclosed mass is calculated to be  $180 M_\odot$ , in a disk property with  $V_{rot} = 6.5$  km s $^{-1}$  and  $r = 3300$  AU. The enclosed mass of  $\geq 180 M_\odot$  is still somewhat large as a single high-mass protostar. Therefore, we conclude that the scenario that methanol masers trace a disk around a protostar is less likely to account for the observed characteristics of the methanol maser emission.

We acknowledge the referee, Anna Bartkiewicz, for careful reading and her constructive suggestions. We also express our appreciation to Vincent Minier for informing us of his results. The JVN project is led by the National Astronomical Observatory of Japan (NAOJ), which is a branch of the National Institutes of Natural Sciences (NINS), Hokkaido University, Ibaraki University, University of Tsukuba, Gifu University, Osaka Prefecture University, Yamaguchi University, and Kagoshima University, in cooperation with the Geographical Survey Institute (GSI), the Japan Aerospace Exploration Agency (JAXA), and the National Institute of Information and Communications Technology (NICT). We are grateful to all staff members of JVN for supporting our observations.

## References

- Bartkiewicz, A., Szymczak, M., van Langevelde, H. J. 2005, *A&A*, 442, L61
- Bartkiewicz, A., Szymczak, M., van Langevelde, H. J., Richards, A. M. S.; Pihlström, Y. M. 2009, *A&A*, 502, 155
- Cragg, D. M., Sobolev, A. M., Godfrey, P. D. 2005, *MNRAS*, 360, 533
- Caswell, J. L., Vaile, R. A., Ellingsen, S. P., Whiteoak, J. B., Norris, R. P. 1995, *MNRAS*, 272, 96
- De Buizer, J. M. 2003, *MNRAS*, 341, 277
- De Buizer, J. M., Bartkiewicz, A., & Szymczak, M. 2012, *ApJ*, 754, 149
- Diamond, P.J., 1995, in ASP Conf. Ser. 82, Very Long Baseline Interferometry and the VLBA, ed. J.A. Zensus, P.J. Diamond, & P.J. Napier (San Francisco: ASP), 227
- Dodson, R., Ojha, R., Ellingsen, S. P. 2004, *MNRAS*, 351, 779
- Eiroa, C., Casali, M. M., Miranda, L. F., Ortiz, E. 1994, *A&A*, 290, 599
- Eiroa, C., Casali, M. M. 1995, *A&A*, 303, 87
- Genzel, R., Downes, D., 1977, *A&AS*, 30, 145
- Goddi, C., Moscadelli, L., Sanna, A., 2011, *A&A*, 535, L8
- Goedhart, S., Gaylard, M. J., van der Walt, D. J. 2004, *MNRAS*, 355, 553
- Heydari-Malayeri, M., Testor, G., Baudry, A., Lafon, G., de La Noe, J., 1982, *A&A*, 113, 118
- Honma, M. et al. 2007, *PASJ*, 59, 88
- Jiang, Z. et al. 2003, *ApJ*, 596, 1064
- Kawaguchi, N., Kobayashi, H., Miyaji, T., Mikoshiba, H., Tojo, A., Yamamoto, Z., Hirose, H. 1994, in VLBI Technology Progress and Future Observational Possibilities, ed. T. Sasao, S. Manabe, O. Kameya, M. Inoue (Tokyo: Terra Scientific Publishing Company), 26
- Matsumoto, N., Honma, M., Isono, Y., Ujihara, H., Kimura, K., Matsumoto, K., Sawada-Satoh, S., Doi, A., Fujisawa, K., Ueno, Y., *PASJ*, 63, 1345
- Menten, K. M. 1991, *ApJ*, 380, L75
- Minier, V., Booth, R. S., Conway, J. E. 2000, *A&A*, 362, 1093 (M00)
- Minier, V., Ellingsen, S. P., Norris, R. P., Booth, R. S. 2003, *A&A*, 403, 1095
- Moscadelli, L.; Cesaroni, R.; Rioja, M. J.; Dodson, R.; Reid, M. J. 2011, *A&A*, 526, A66
- Nagayama, T. et al. 2008 *PASJ*, 60, 1069
- Norris, R. P., Byleveld, S. E., Diamond, P. J., Ellingsen, S. P., Ferris, R. H., Gough, R. G., Kesteven, M. J., McCulloch, P. M., Phillips, C. J., Reynolds, J. E., Tzioumis, A. K., Takahashi, Y., Troup, E. R., Wellington, K. J. 1998, *ApJ*, 508, 275
- Phillips, C. J., Norris, R. P., Ellingsen, S. P., McCulloch, P. M. 1998, *MNRAS*, 300, 1131
- Rygl, K. L. J., Brunthaler, A., Reid, M. J., Menten, K. M., van Langevelde, H. J., Xu, Y. 2010, *A&A*, 511, A2
- Sanna, A., Moscadelli, L., Cesaroni, R., Tarchi, A., Furuya, R. S., Goddi, C. 2010a, *A&A*, 517, A71
- Sanna, A., Moscadelli, L., Cesaroni, R., Tarchi, A., Furuya, R. S., Goddi, C. 2010b, *A&A*, 517, A78
- Shibata, K. M., Kameno, S., Inoue, M., Kobayashi, H. 1998, in Radio Emission from Galactic and Extragalactic Compact Sources, ASP Conference Series, Volume 144, IAU Colloquium 164, eds. J.A. Zensus, G.B. Taylor, & J.M. Wrobel p. 413.
- Sugiyama, K., Fujisawa, K., Doi, A., Honma, M., Kobayashi, H., Bushimata, T., Mochizuki, N., Murata, Y. 2008, *PASJ*, 60, 23
- Sugiyama, K., Fujisawa, K., Doi, A., Honma, M., Isono, Y., Kobayashi, H., Mochizuki, N., Murata, Y. 2008, *PASJ*, 60, 1001
- Sugiyama, K., Fujisawa, K., Doi, A., Honma, M., Isono, Y., Kobayashi, H., Mochizuki, N., Murata, Y., Sawada-Satoh, S., Wajima, K. 2011, *PASJ*, 63, 53
- Szymczak, M., Hrynek, G., Kus, A. J. 2000, *A&AS*, 143, 269
- Torstensson, K. J. E., van Langevelde, H. J., Vlemmings, W. H. T., Bourke, S. 2011, *A&A*, 526, A38
- Walsh, A. J., Hyland, A. R., Robinson, G., Burton, M. G. 1997, *MNRAS*, 291, 261
- Walsh, A. J., Burton, M. G., Hyland, A. R., Robinson, G. 1998, *MNRAS*, 301, 640
- Wouterloot, J.G.A., Brand, J., 1989, *A&AS*, 80, 149
- Wynn-Williams, C. G., Becklin, E. E., Neugebauer, G. 1974a, *ApJ*, 187, 473
- Wynn-Williams, C. G., Werner, M. W., Wilson, W. J. 1974b, *ApJ*, 187, 41
- Xu, Y., Li, J. J., Hachisuka, K., Pandian, J. D., Menten, K. M., Henkel, C. 2008, *A&A*, 485, 729
- Yang, J., Jiang, Z., Wang, M., Ju, B., Wang, H. 2002, *ApJS*, 141, 157